Journal of Luminescence 178 (2016) 226–233

Contents lists available at ScienceDirect

Journal of Luminescence

journal homepage: www.elsevier.com/locate/jlumin

Full Length Article

Broadened band C-telecom and intense upconversion emission of Er^{3+}/Yb^{3+} co-doped $CaYAlO_4$ luminescent material obtained by an easy route

R.V. Perrella [a], M.A. Schiavon [a], E. Pecoraro [b], S.J.L. Ribeiro [b], J.L. Ferrari [a,*]

[a] Grupo de Pesquisa em Química de Materiais – (GPQM), Departamento de Ciências Naturais, Universidade Federal de São João del Rei (UFSJ), Campus Dom Bosco, Praça Dom Helvécio, 74, 36301-160 São João del Rei, MG, Brazil
[b] UNESP, Institute of Chemistry, P.O. Box 355, 14800-970 Araraquara, SP, Brazil

ARTICLE INFO

Article history:
Received 12 January 2016
Received in revised form
11 May 2016
Accepted 30 May 2016
Available online 4 June 2016

Keywords:
Calcium Yttrium Aluminate
Rare earths
Upconversion
C-telecom window

ABSTRACT

This work reports on photoluminescence properties of Er^{3+}/Yb^{3+} co-doped $CaYAlO_4$ in powder form, synthesized by an easy route using citric acid as ligand to form complex precursor. The 1.2 mol% of Yb^{3+} was fixed, while the amount of Er^{3+} changed in 0.5, 1.5 and 3 mol% in order to evaluate the photoluminescence properties as a function of the Er^{3+} concentration. The structural and thermal properties of the viscous solutions and powder materials obtained after the heat-treatment at 1000, 1100 and 1200 °C for 4 h were evaluated by XRD, FTIR and TG/DTA analysis. The results showed the formation of pure $CaYAlO_4$ tetragonal crystalline phase after heat-treatment at 1100 °C and 1200 °C. Intense emission in the visible region under excitation at 980 nm was attributed to upconversion process, from Er^{3+} intra-configurational f–f transitions. The emissions were assigned to the transitions $^2H_{11/2} \rightarrow {}^4I_{15/2}$ and $^4S_{3/2} \rightarrow {}^4I_{15/2}$ (green region), and $^4F_{9/2} \rightarrow {}^4I_{15/2}$ (red region) energy levels. The ratio between emission band integrated areas assigned to the red and green emissions increased as a function of Er^{3+} concentration. Under excitation at 980 nm with 100 mW of power pump, the materials also showed intense and broadening emission with maximum at 1520 nm with FWHM of 84.74 nm for the sample $CaYAlO_4$:1.5% Er^{3+}/1.2% Yb^{3+} heat-treated at 1000 °C for 4 h. The photoluminescence properties showed that these materials are promising for use in C-telecom band as optical amplifier biological marker or/and solid-state laser devices under excitation at 980 nm.

© 2016 Elsevier B.V. All rights reserved.

1. Introduction

Photoluminescent materials are typically composed by inorganic solids, consisting of a host matrix and small amounts of impurities intentionally added in order to give rise to the emission of radiation in specific regions of the electromagnetic spectrum. Among those impurities are the rare earth ions (RE^{3+}) [1–10]. The photoluminescent properties of RE^{3+} come from the splitting of 4f levels assigned to the inter-electronic interactions, the spin-orbit coupling and the ligand field effect on these ions, when they are present in a host matrix [11].

Among the RE^{3+} most extensively studied in recent years, Er^{3+} plays a central role, since its spectroscopic properties allow it application in several technological devices. The intense emission in the near infrared region around 1550 nm presented by Er^{3+}, under excitation at 980 nm, enables the development of optical amplifiers operating at C-band telecommunications (1520–1570 nm), which corresponds to the region with the lower energy loss in silicate based materials [12–15]. Furthermore, the full-width at half maximum (FWHM) of the emission band around 1550 nm is an important spectroscopic parameter. Manzani et al. prepared optical fibers based on tellurite glasses, with base composition of $70TeO_2$–$15GeO_2$–$5K_2O$–$10Bi_2O_3$ and obtained high FWHM, about 92 nm [16]. Filho et al. obtained a FWHM of 53 nm for the ternary system Al_2O_3–SiO_2–GeO_2 synthesized from the modified Pechini's method [14].

Apart from the characteristic emission of the Er^{3+} around 1550 nm, emissions in visible region resulting from energy transfer mechanisms, such as energy upconversion (UC) upon excitation in the near infrared (980 nm) can be detected. This process allows the development of bio-photonic materials used in biological labeling [17,18], shorter wavelength solid-state lasers, operating in the visible region under excitation in the near infrared [19,20], and increase the efficiency of energy conversion devices such as solar cells [21,22]. Some studies reported in the literature regard UC in doped materials containing only Er^{3+} [23]. However,

* Corresponding author. Tel./fax: +55 32 3379 2481.
E-mail addresses: ferrari@ufsj.edu.br, jeffersonferrari@gmail.com (J.L. Ferrari).

http://dx.doi.org/10.1016/j.jlumin.2016.05.056
0022-2313/© 2016 Elsevier B.V. All rights reserved.

due to its small absorption cross-section, [25] Yb^{3+} has been used as a sensitizer, efficiently absorbing energy at 980 nm and transferring it to a neighboring Er^{3+}.

As energy transfer processes and photoluminescence are dependent on distance between the neighboring of RE^{3+} and the composition and structure of the host matrix in which these ions are allocated, the choice of a suitable host matrix becomes of great importance. Among the main features that a host must present stand out: good solubility of RE^{3+}; chemical and thermal stability; and especially low phonon's energy. A host that meets these requirements is $CaYAlO_4$. Such crystalline compound presents low phonon´s energy, around 322 cm^{-1} [24], that is lower than in others hosts, such as $NaGd(WO_4)_2$, and $NaY(MoO_4)_2$ (around 900 cm^{-1}) [25,26], $LaPO_4$ (about 1050 cm^{-1}) [27] and YVO_4 (890 cm^{-1}) [28]. It has a tetragonal structure formed by $[AlO_6]^{3-}$ octahedron presenting an inversion center *i*, while the Ca^{2+} and Y^{3+} are randomly located over the same sites of C_{4v} symmetry [29–32]. This random distribution of ions with different charges creates an inhomogeneous environment so that the RE^{3+} spectra occupying the positions of Y^{3+} in the $CaYAlO_4$ structure generally exhibit broad bands. This feature is particularly important for the emission in the region of 1550 nm for Er^{3+}. Furthermore, this matrix is more stable than sulfides, fluorides or nitrides and presents good thermal and mechanical properties, which make it a great candidate for use in lasers biological markers and others optical applications. The thermal expansion coefficients of $CaYAlO_4$ in the range from 20 to 1200 K are $8 \times 10^{-6}\ K^{-1}$ and $11 \times 10^{-6}\ K^{-1}$ for the *a*- and *c*-axis, respectively. The Mohs hardness is around 6 [32].

Some works in the literature have described the use of $CaYAlO_4$ as host of Er^{3+} with potential application in photonic devices prepared from Czochralski method [33]. Souriau et al. described the spectroscopic behavior of single crystals of $CaYAlO_4$: Er^{3+}/Yb^{3+} obtained by means of this technique [34]. Lv et al. obtained single crystals of $CaYAlO_4$:Ho^{3+}/Er^{3+} and $CaYAlO_4$:Eu^{3+}/Er^{3+} and carried out a study on application of this system as laser in the medium infrared region, around 2.7 μm [24]. Zhou et al. synthesized a single crystal of $CaYAlO_4$:Er^{3+} and analyzed their spectroscopic properties in the visible and infrared region [29]. However, to the best of our knowledge, there is no report in the literature that describes the obtaining of $CaYAlO_4$:Er^{3+}/Yb^{3+} from the complexing of cations in solution, using citric acid as ligand. This chemical route allows a good homogenization of the precursor solution, due to the ease complexation of metals with citric acid, besides presenting a low cost of synthesis [35–37].

Therefore, this paper presents on synthesis of $CaYAlO_4$ containing Er^{3+} and Yb^{3+} in different concentrations, based on the use of citric acid to form complexes precursors. The study of the photoluminescence and structural properties of these materials were performed and related to the concentration of RE^{3+} and to the different heat-treatment temperatures.

2. Experimental

The starting materials for the synthesis of $CaYAlO_4$: *X*% Er^{3+}/1.2% Yb^{3+} (where $X=0.5$, 1.5 and 3) included Y_2O_3, Er_2O_3 and Yb_2O_3 (Aldrich −99.999%), $CaCO_3$ (Dynamic −99%), $Al(NO_3)_3.9H_2O$ (Synth −99%) and citric acid (Dynamic −99.5%). All reagents were used without further purification. The experimental procedure was based on previous work of our group [38]. Initially, stoichiometric amounts of Y_2O_3, $CaCO_3$ and $Al(NO_3)_3.9H_2O$ were solubilized separately in 1 mol L^{-1} HCl solutions and subsequently transferred to a single beaker. The Er_2O_3 and Yb_2O_3 were also solubilized in aqueous solutions of hydrochloric acid (1 mol L^{-1}), and then, standardized at room temperature by titration with EDTA (0.01 mol L^{-1}). Next, an exact volume of each solution containing corresponding RE^{3+}, to get materials with changing of Er^{3+} and Yb^{3+} concentration was pipetted into the beaker containing the Y^{3+}, Ca^{2+} and Al^{3+} solubilized. After, the mass of citric acid corresponding 5 times to the total number of moles of metals in solution was dissolved in deionized water and transferred to the beaker containing the Y^{3+}, Ca^{2+}, Al^{3+}, Er^{3+} and Yb^{3+} to form the citrate complexes precursors. The complexes solutions were kept under magnetic stirring at 70 °C for 6 h, which leads to an increasing of solutions viscosities. For each concentration of Er^{3+}, one viscous solution was prepared. It is noteworthy the viscous solutions were obtained carefully so, they presented the same visual aspect. Then, all viscous solutions were calcined at 200 °C for 4 h and 400 °C for 4 h to dry the precursor. The precursors obtained were fully ground in agate mortar and heat-treated at 1000, 1100 and 1200 °C in air atmosphere for 4 h to obtain the materials in powder form.

The viscous solutions obtained were submitted to thermogravimetric analysis (TG) and differential thermal analysis (DTA) by using a thermobalance Shimadzu model DTG −60 H, from room temperature up to 1100 °C, with heating rate of 10 °C min^{-1} under air atmosphere. The crystalline structure was evaluated by means of X-ray diffraction (XRD) by a Shimadzu XRD 6000 diffractometer with Cu Kα radiation ($\lambda=1.5418$ Å), graphite monochromator, scan speed of 0.75 deg. min^{-1} with 2θ ranging from 20° to 80°. Fourier Transform Infrared Spectroscopy (FTIR) was performed by a spectrophotometer Perkin Elmer Spectrum GX. The samples were processed in pellets diluted in KBr and kept under pressure of 10*t* for 1 min. The spectra were obtained between 4000 and 400 cm^{-1} range with 4 cm^{-1} of resolution. The emission spectra between 1400 and 1700 nm of the $CaYAlO_4$ samples containing Er^{3+} and Yb^{3+} were recorded by using a Fluorolog Horiba Jobin Yvon, with an InGaAs detector sensitive from 800 to 1700 nm with excitation at 980 nm using fiber couple laser diode with 100 mW of power. The upconversion emission spectra in the region between 500 and 700 nm were carried out in the same spectrometer; however a photomultiplier tube was used to monitor the emission in visible range. A diode laser operating at 980 nm was used as an excitation source, varying the power excitation from 100 to 500 mW with steps of 100 mW.

3. Results and discussion

The viscous solutions obtained as precursor of the materials were submitted to TG and DTA analysis to investigate the thermal decomposition profiles and thermal stability of the materials. Fig. 1 shows the thermograms of the samples containing *X* mol% of Er^{3+} (where $X=0.5$, 1.5 and 3) and 1.2 mol% of Yb^{3+}. According to the results, all solutions showed a similar thermal decomposition profile, with mass losses occurring in three distinct steps. The first one occurs from room temperature to about 160 °C, that is related to the dehydration of viscous solutions and to losses of citric acid uncomplexed [35,36], corresponding to approximately 54% of the mass losses. Next, takes place a mass loss between 160 °C and 250 °C, which could be assigned to the beginning of thermal decomposition of the metal-citrate species [37], as shown by small endothermic event at 195 °C. This step corresponds to losses of mass of approximately 25%. The last loss of mass, approximately 18%, which occurs from 360 °C, is associated to the organic matter oxidation [35–37], as can be seen by the presence of exothermic peaks between 400 °C and 566 °C. The final yield of thermal decomposition is around 3% of the initial mass used in the analysis. This low value is associated to the large amount of citric acid regarding to the amount of metals in solution. This procedure was performed to promote better homogeneity of ions distribution

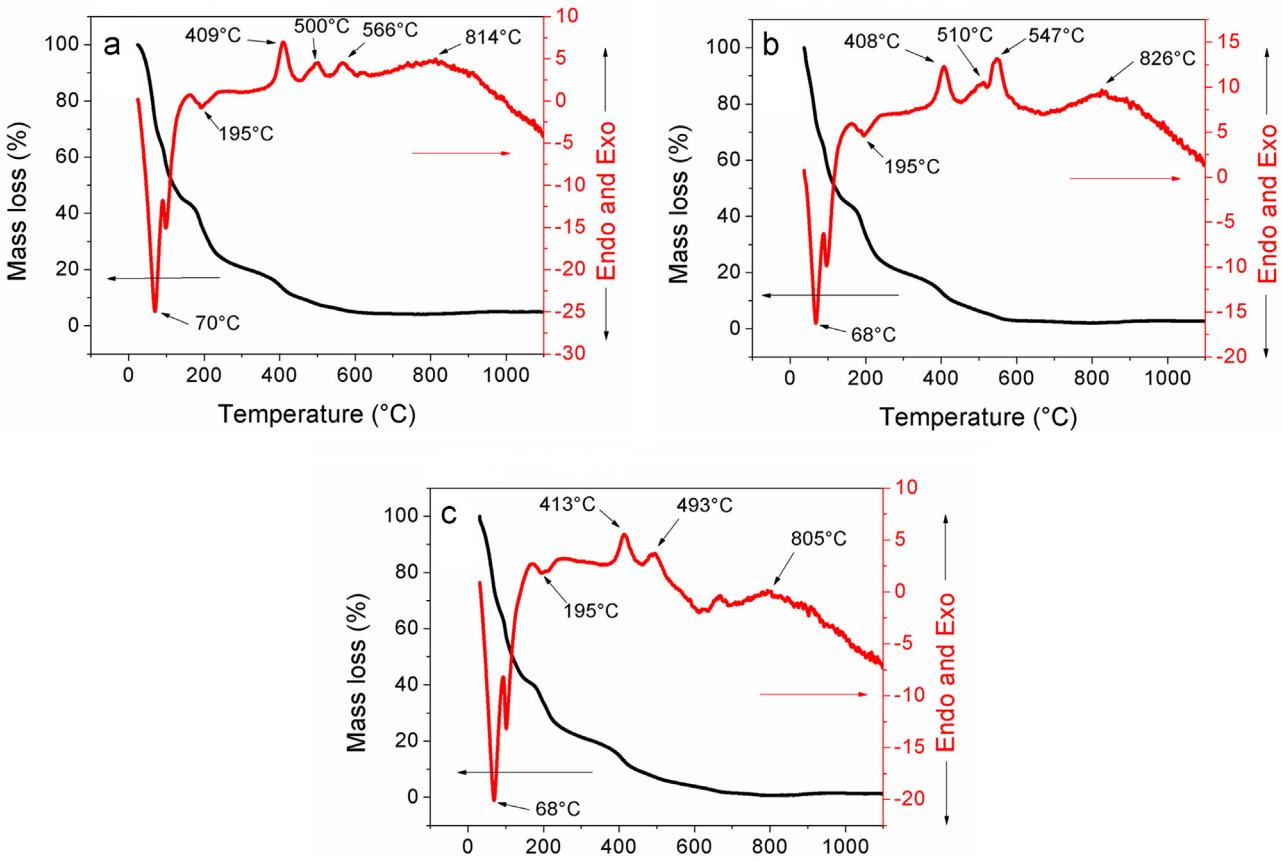

Fig. 1. TG and DTA analysis of the viscous solutions containing (a) 0.5 mol%, (b) 1.5 mol% and (c) 3 mol% of Er^{3+} and 1.2 mol% of Yb^{3+}.

present in the precursor solution carefully prepared. Above 800 °C several exothermic events occurs without any corresponding mass loss, which can be associated to the beginning of $CaYAlO_4$ nucleation stage of particles. Based on results observed in the TG and DTA analysis, all viscous solutions were calcined at 200 °C for 4 h and 400 °C for 4 h, followed by heat-treatment at 1000, 1100 and 1200 °C for 4 h to obtain $CaYAlO_4$ containing Er^{3+} and Yb^{3+}.

Fig. 2 shows XRD patterns of the materials obtained after the heat-treatment at 1000, 1100 and 1200 °C for 4 h. The results show the formation of the $CaYAlO_4$ with tetragonal crystal structure belonging to the space group I4/mmm, according to database code ICSD: 72104. Only XRD patterns of the materials heat-treated at 1000 °C for 4 h (Fig. 2a) it is possible to observe the presence of diffraction peaks that are not assigned to $CaYAlO_4$ structure. These peaks indicate the presence of crystalline structure, known as the secondary phase, and assigned to the monoclinic structure of $Y_4Al_2O_9$ (ICSD 63650).

Meanwhile, the samples heat-treated at 1100 and 1200 °C do not show peaks assigned to the secondary phase, indicating that the presence of secondary phases was reduced. Only peaks corresponding to the pure $CaYAlO_4$ structure were observed. The volume of crystallinity amount of all samples increases as a function of heat-treatment temperature. No diffraction peak attributed to any phase containing erbium or ytterbium, as Er_2O_3 or Yb_2O_3, was detected, indicating the insertion of RE^{3+} in the crystal structure of $CaYAlO_4$. As suggested by Kustov et al. [32] and Geng et al. [39] Y^{3+} can be replaced by RE^{3+} in the C_{4v} symmetry sites, this substitution is favored by the fact that Er^{3+}, Yb^{3+} and Y^{3+} have similar ionic radii, 1.144, 1.125 and 1.159 Å, respectively, and same number of oxidation. Another type of insert which cannot be completely disregarded is the location of RE^{3+} within the interstices of the crystalline structure.

Fig. 3 shows the FTIR spectra of citric acid, viscous solution obtained during the synthesis and $CaYAlO_4$:1.5% Er^{3+}/1.2% Yb^{3+} heat-treated at 1000, 1100 and 1200 °C for 4 h. It is important to observe that all the samples heat-treated showed same characteristic bands in the FTIR spectra and any change in position of bands was not observed by varying the concentration of Er^{3+}. We observe that the bands assigned to citric acid are also present in the spectrum of the viscous solutions, which confirm the presence of citrate molecules unalloyed. The stretching of O–H bonds appears at 3343 cm^{-1}. The band around 1740 cm^{-1} may be attributed to the stretching of C=O groups, while C–O group stretching band can be observed at 1113 cm^{-1} [40]. Bands between 473 and 811 cm^{-1} are assigned to the stretching of the metal–oxygen bonds. The band around 809 cm^{-1} may be attributed to the stretching of the Al–O bonds [41], while the band around 473 cm^{-1} is attributable to vibration of Y–O bonds [42]. These vibrations confirm the presence of metal–oxygen bonds present in $CaYAlO_4$ structure. The FTIR spectra of the samples after the heat-treatments indicate that the carbonates and O–H groups, derived from citric acid and water, decrease as the annealing temperature increases. Full elimination of these organic groups is very important for the photoluminescence processes, because these species act as fluorescence-quenching centers, due to their vibration frequencies. For example, O–H elimination is very important for those materials which exhibit emission around 1550 nm, once the energy of only two vibrations of O–H groups is enough to deactivate the $^4I_{13/2}$ excited state of Er^{3+}, which leads to a suppression of the emission due to non-radiative decay by multiphonon relaxation [43].

The upconversion (UC) emission spectra of the samples heat-treated at 1200 °C are shown in Fig. 4. The analyzes were performed in the visible region, specifically between 500 and 700 nm using

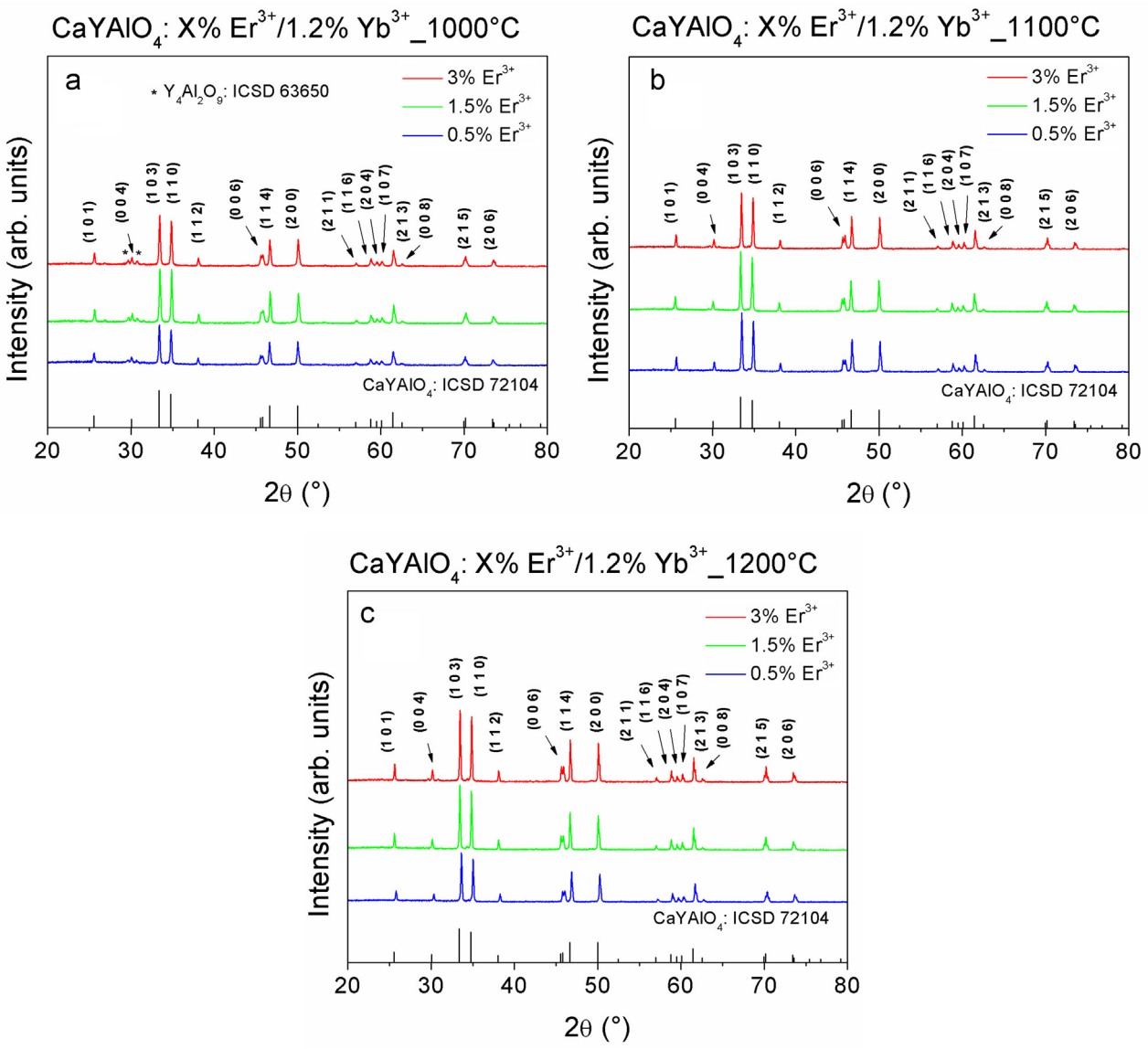

Fig. 2. The XRD patterns of the samples obtained after the heat-treatment at (a) 1000, (b) 1100 and (c) 1200 °C for 4 h in air atmosphere.

excitation at 980 nm and power excitation from 100 up to 500 mW, with steps of 100 mW. All emissions observed are attributed to the intraconfigurational f–f transitions of Er^{3+}. In all emission spectra, it can be observed basically the presence of three bands, two in the green region ($^2H_{11/2} \rightarrow {}^4I_{15/2}$ and $^4S_{3/2} \rightarrow {}^4I_{15/2}$), with maximum emission peak at 529 and 550 nm, respectively, and another in the red region, with a maximum emission peak at 663 nm, attributed to the transition $^4F_{9/2} \rightarrow {}^4I_{15/2}$. A behavior observed for all samples is that the emission in the green region is more intense than the emission in the red region. Furthermore, it is possible to observe that, increasing the concentration of Er^{3+} leads to an increase of emission attributed to the transition $^4F_{9/2} \rightarrow {}^4I_{15/2}$, relative to the emission assigned to transitions $^2H_{11/2} \rightarrow {}^4I_{15/2}$ and $^4S_{3/2} \rightarrow {}^4I_{15/2}$.

A comparative UC emission spectrum between samples with different concentrations of Er^{3+} was also performed. As can be seen in Fig. 5, the UC emission intensity gradually increases with increasing concentration of Er^{3+}. The highest UC emission intensity was achieved for the sample containing 3 mol% of Er^{3+}. This same behavior was observed in all powers excitation. This may suggest that UC emission efficiency increases with increasing concentration of Er^{3+}.

The relationship between the area of each UC emission and the pump power helps us to understand the mechanisms of energy transfer and identify the number of photons involved in the absorption process. The area of the UC emissions band is related to the power excitation pump according to $I \propto P^n$, where I is the area of UC emission, P is the power of the excitation source and n is the number of photons involved in the excitation process [44]. The number of photons (n) is deduced by means of the slope of the curve log (I) versus log (pump power). Fig. 6 shows the logarithmic plots of the integrated area of the emissions as function of the excitation power for $CaYAlO_4$:3% Er^{3+}/1.2% Yb^{3+} heat-treated at 1200 °C. The slope of the green emission was 1.94, whereas the slope for the red emission was 1.98, indicating that two photons need to be absorbed for generating the emission in different regions. Both linear adjustments showed excellent correlation coefficients R, around 0.999.

For UC to occur it is necessary that the excited levels $^2H_{11/2}$, $^4S_{3/2}$ and $^4F_{9/2}$ are populated. The two most common excitation mechanisms involved in UC are Excited State Absorption (ESA) and the Energy Transfer Upconversion (ETU) [45]. Fig. 7 shows the energy levels diagram for Er^{3+} and Yb^{3+} and the mechanisms involved in the UC process. The ESA involves the absorption of one photon by an Er^{3+}, promoting the electronic excitation from the ground state $^4I_{15/2}$, to the excited state $^4I_{11/2}$, in a process known as

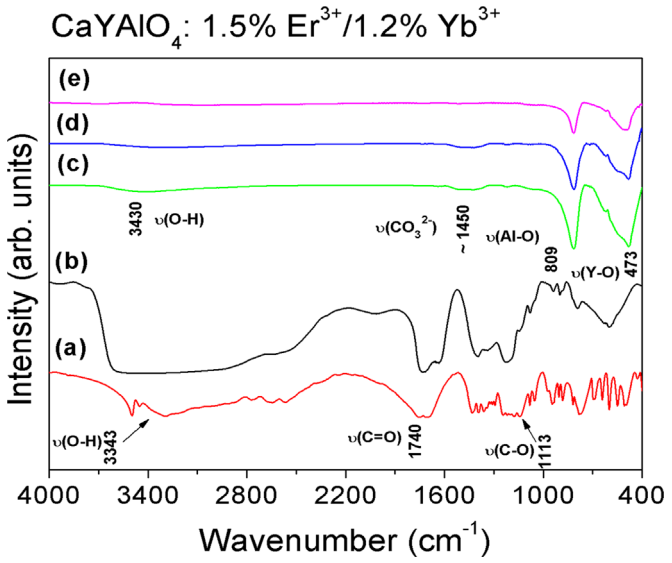

Fig. 3. FTIR analysis of (a) citric acid, (b) viscous solution and the synthesized $CaYAlO_4$:1.5% Er^{3+}/1.2% Yb^{3+} after heat-treatment at (c) 1000, (d) 1100 and (e) 1200 °C for 4 h in air atmosphere.

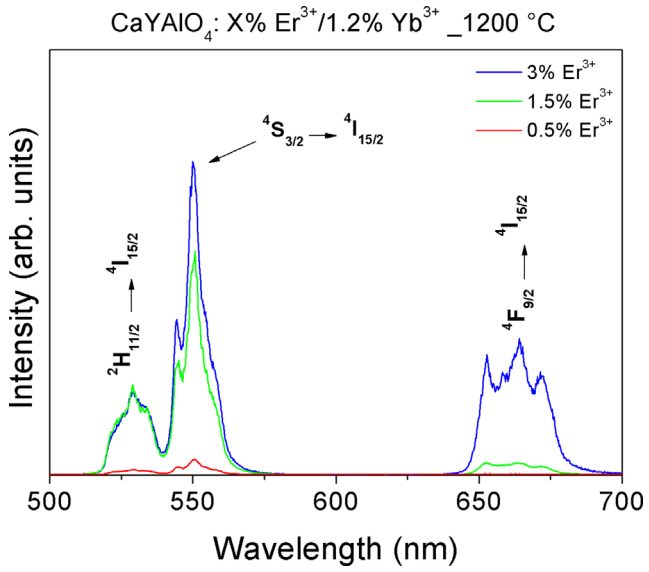

Fig. 5. UC emission spectrum of samples with different concentrations of Er^{3+} heat-treated at 1200 °C. The excitation power was 100 mW.

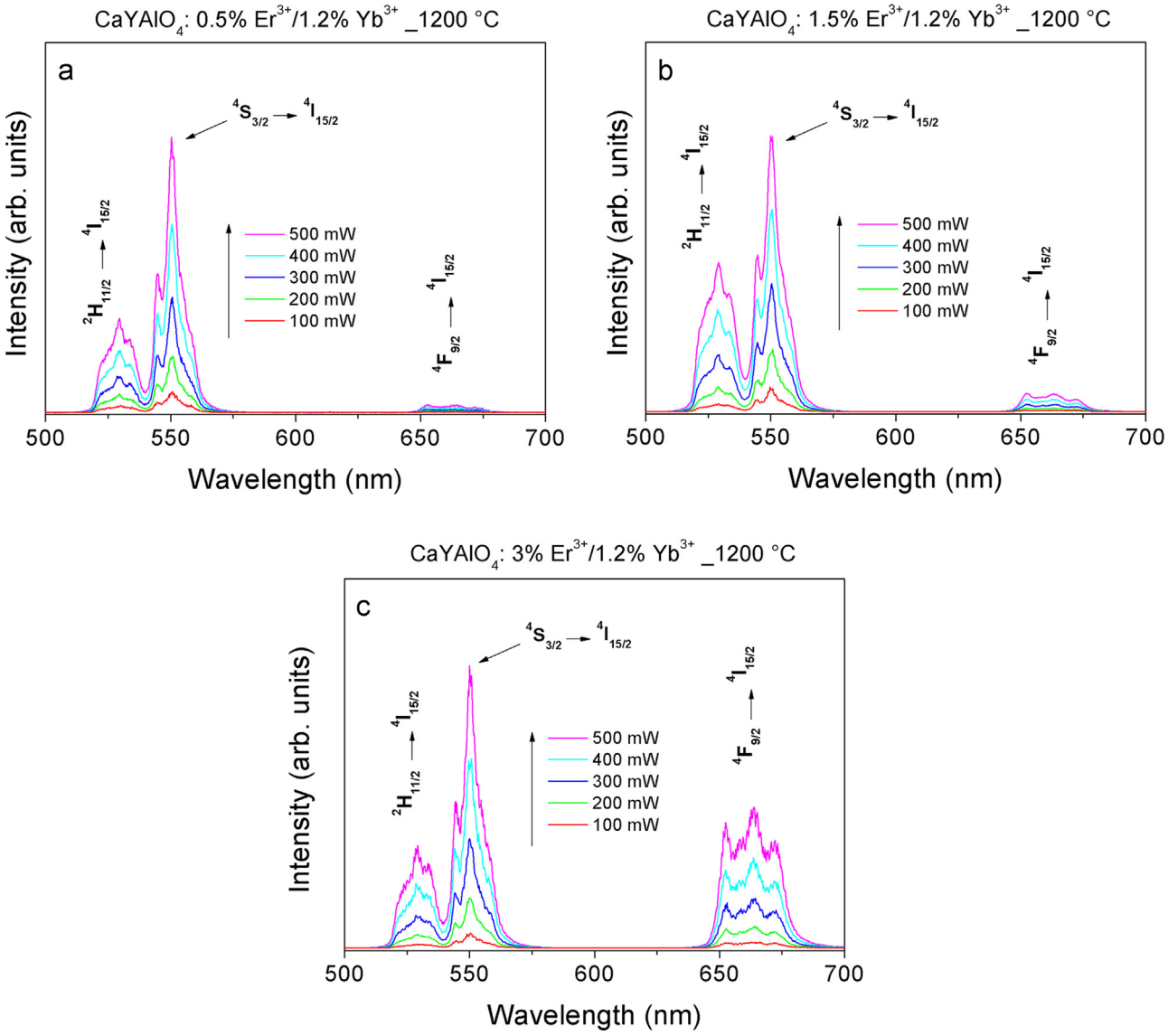

Fig. 4. UC emission spectra of $CaYAlO_4$:Er^{3+}/Yb^{3+} samples heat-treated at 1200 °C with different concentrations of Er^{3+}: (a) 0.5 mol%, (b) 1.5 mol% and (c) 3 mol%.

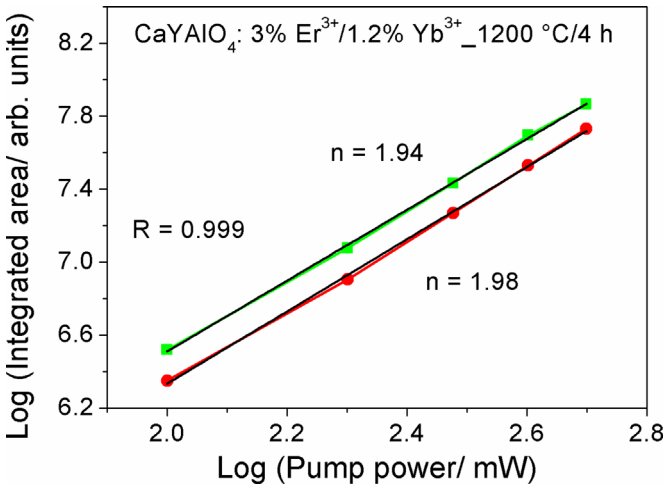

Fig. 6. Dependence of upconversion emission intensities for Er^{3+}/Yb^{3+} co-doped $CaYAlO_4$ as a function of power pump at 980 nm.

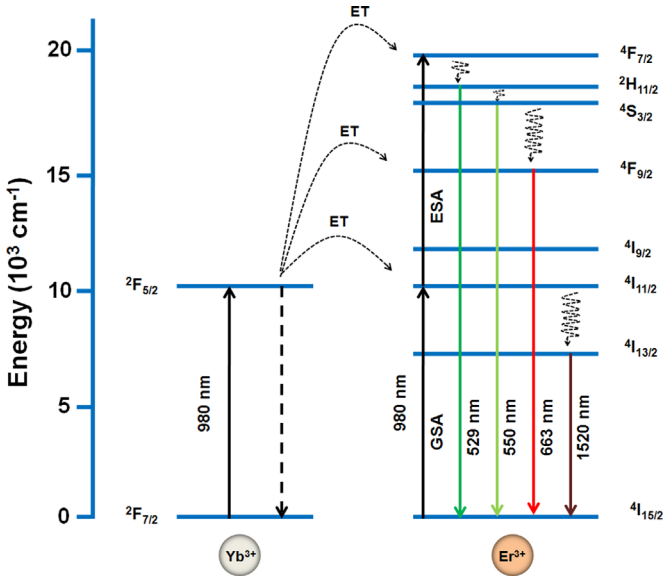

Fig. 7. Energy levels diagram of Er^{3+} and Yb^{3+} with the characteristics ETU, ESA and UC emissions in $CaYAlO_4$under excitation at 980 nm.

Ground State Absorption (GSA). Due to the long lifetime of the excited state $^4I_{11/2}$, another photon can be absorbed by the Er^{3+} and a population inversion can be promoted, causing more energetic levels, such as the $^4F_{7/2}$, being populated. Later, through non-radiative decays, the Er^{3+} can decay to the excited levels $^2H_{11/2}$, $^4S_{3/2}$ and $^4F_{9/2}$ and, from there, emitting light at 529, 550 and 663 nm, respectively. On the other hand, ETU is a process in which energy transfer occurs between two close ions. In this case, Yb^{3+} acts as a sensitizer and absorbs radiation at 980 nm from the excitation laser, more efficiently than Er^{3+}, once its absorption cross-section at 980 nm is higher than that for Er^{3+}. Then, by decaying, the excited state $^2F_{5/2}$ of Yb^{3+} transfers its energy to $^4I_{11/2}$ level of Er^{3+}. This process is possible due to the fact that these two levels are resonant in terms of energy. Next, a second photon promotes the electronic excitation of Er^{3+} from the level $^4I_{11/2}$ up to more energetic states, such as $^4F_{7/2}$. Finally, in the same way as it happens for the ESA, those high energy levels can decay for lower levels by non-radiative processes, leading to light emission from the states $^2H_{11/2}$, $^4S_{3/2}$ and $^4F_{9/2}$. According to Anderson et al., ETU process is more efficient than ESA process [46], and with the presence of the Yb^{3+} as sensitizers to transfer energy to Er^{3+}, ETU is certainly prevailing mechanism in this system.

As previously noted, all materials showed emission mainly in the green region, and with increasing concentration of Er^{3+}, there is an increase in the ratio between the area of the band attributed to the emission in the red region ($^4F_{9/2}\rightarrow{}^4I_{15/2}$) and the emissions in the green region ($^2H_{11/2}\rightarrow{}^4I_{15/2}$ and $^4S_{3/2}\rightarrow{}^4I_{15/2}$). This may be associated with the presence of RE^{3+} on the surface of the crystals, which would allow the increase of non-radiative mechanisms by clustering. Thus, the non-radiative processes between the transitions $^4F_{7/2}\rightarrow{}^4F_{9/2}$, $^2H_{11/2}\rightarrow{}^4F_{9/2}$ and $^4S_{3/2}\rightarrow{}^4F_{9/2}$ may occur more intensely for higher concentrations of Er^{3+}, which increases the transition $^4F_{9/2}\rightarrow{}^4I_{15/2}$ attributed to the emissions in the red

Table 1
Values of the FWHM (nm) of the emission assigned to the $^4I_{13/2}\rightarrow{}^4I_{15/2}$ of the Er^{3+}.

1000 °C		1200 °C	
% of Er^{3+}	FWHM (nm)	% of Er^{3+}	FWHM (nm)
0.5	72.12	0.5	68.59
1.5	84.74	1.5	67.51
3	69.82	3	64.42

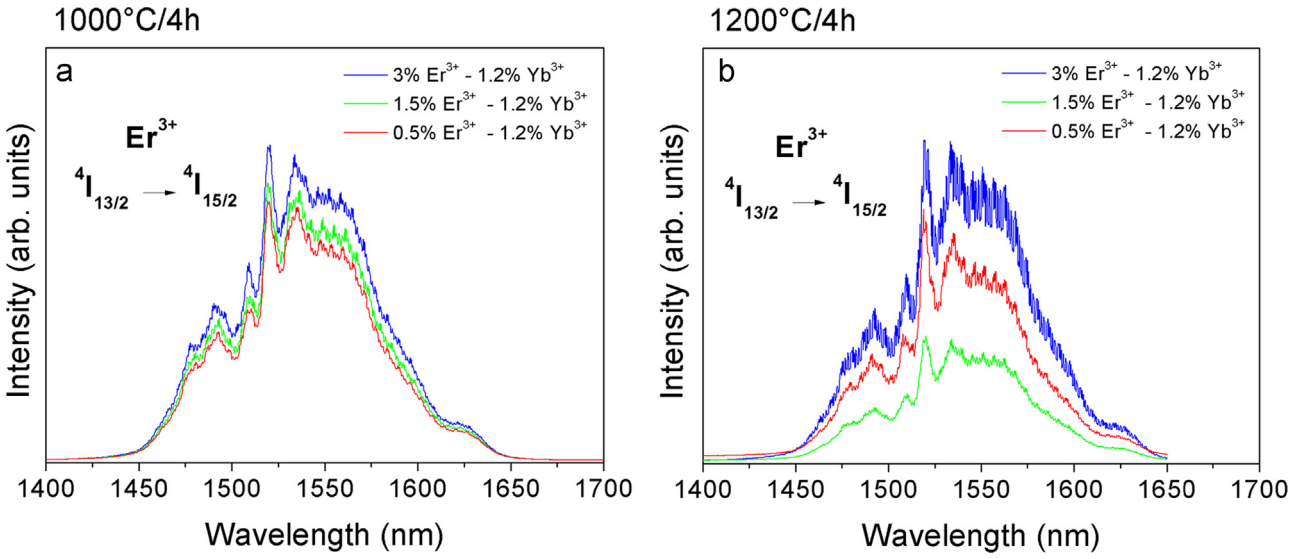

Fig. 8. Infrared emission of Er^{3+}/Yb^{3+} co-doped $CaYAlO_4$ obtained at (a) 1000 and (b) 1200 °C under excitation at 980 nm fixing the power source at 100 mW.

region. Furthermore, as shown by FTIR, organic groups, such as O–H, which promote an increase of non-radiative processes, are virtually eliminated during the heat-treatment process, which implies that, the increasing of the intensity for red emissions is associated with a reduction of the distances between the RE^{3+}, by the increasing of their concentration.

Fig. 8 shows the emission spectra from 1400 to 1700 nm, for samples heat-treated at 1000 °C and 1200 °C under excitation at 980 nm with 100 mW of power. All samples showed intense emission in the near infrared region, with maximum peak emission at 1520 nm, attributed to the transition $^4I_{13/2} \rightarrow {}^4I_{15/2}$ of Er^{3+}. This emission presents great technological interest, once these materials could find applications as optical amplifiers for C-telecom band. Under excitation at 980 nm, Yb^{3+} undergoes an electronic excitation from its ground state $^2F_{7/2}$ to the excited state $^2F_{5/2}$. This follows energy transfer to the state $^4I_{11/2}$ of Er^{3+}. From there and through non-radiative decay processes the $^4I_{13/2}$ state can be populated, giving rise to the emission around 1520 nm. An interesting result observed for all samples is the broadening of the emission bands in that region. Table 1 shows the values of FWHM calculated for samples heat-treated at 1000 and 1200 °C. The values are between 64.62 and 84.74 nm. It is possible to observe that the increase of the heat-treatment temperature causes a reduction in the FWHM values, indicating that the symmetry around Er^{3+} becomes less distorted.

The values of FWHM of the emission around 1520 nm presented here are higher than those reported by some systems containing binary and ternary oxides, such as SiO_2–HfO_2 (FWHM = 50 nm) [47] and SiO_2–Al_2O_3–GeO_2 (FWHM = 53 nm) [14] and of the same order of magnitude to other binary systems such as Ta_2O_5–SiO_2 (FWHM = 92 nm) [48] and glasses tellurium-based (FWHM = 92 nm) [16] and tellurium and tungsten based (FWHM = 77 nm) [49]. In those systems the enlargement of the band emission can be associated to the inhomogeneous environment of Er^{3+}, resulting in broadened emission bands in the near infrared region. In the case of $CaYAlO_4$, it is no different. As previously discussed, in its crystalline structure, the Y^{3+} and Ca^{2+} are randomly positioned on equivalent sites of C_{4v} symmetry. Thus, when Er^{3+} is added in the crystal structure and occupies the Y^{3+} position, the non-homogeneous environment caused by differences in charge of the Y^{3+} and Ca^{2+} may cause a broadening of the emission band in the region around 1520 nm. Such broadening makes this a promising material for use in optical amplifiers operating in the third telecommunications window and in energy conversion devices, such as solar cells as well.

4. Conclusions

In summary, $CaYAlO_4$:Er^{3+}/Yb^{3+} photoluminescent co-doped material was successfully synthesized by using citric acid as a ligand to form complex solution precursor. The XRD results showed that pure $CaYAlO_4$ phase could be obtained after the heat-treatment at 1100 and 1200 °C for 4 h. All obtained compositions showed intense UC emission under excitation at 980 nm, with bands centered at 529, 550 and 663 nm, attributed to the transitions $^2H_{11/2} \rightarrow {}^4I_{15/2}$, $^4S_{3/2} \rightarrow {}^4I_{15/2}$ and $^4F_{9/2} \rightarrow {}^4I_{15/2}$, respectively. Although the UC emission in the green region had been more intense than UC emission in the red region, it was observed that with increasing concentration of Er^{3+} there is an increase in the ratio between the area of the bands attributed to the emission in the red region ($^4F_{9/2} \rightarrow {}^4I_{15/2}$) and the emissions in the green region ($^2H_{11/2} \rightarrow {}^4I_{15/2}$ and $^4S_{3/2} \rightarrow {}^4I_{15/2}$), indicating that there is an intensification of the non-radiative decay mechanisms with increasing of Er^{3+} concentration. The samples also showed intense emission located around 1520 nm, attributed to the transition $^4I_{13/2} \rightarrow {}^4I_{15/2}$, with FWHM up to 84.74 nm for $CaYAlO_4$:1.5% Er^{3+}/1.2% Yb^{3+} heat-treated at 1000 °C for 4 h. The photoluminescence properties showed by these materials make them promising for use in C-telecom band, biological marker, and energy conversion devices, such as solar concentrators and solid-state lasers.

Acknowledgments

The authors would like to acknowledge FAPEMIG (Projects: APQ-00303-13 and APQ-00901-12), FAPESP, CAPES, and CNPq (Projects: 470157/2013-5 and 305968/2014-9). This work is a collaboration research project of members of the Rede Mineira de Química (RQ-MG) supported by FAPEMIG (Project: CEX - RED-00010-14).

References

[1] G. Rajan, K.G. Gopchandran, Opt. Mater. 32 (2009) 121.
[2] Z.J. Li, Y.J. Zhang, H.W. Zhang, H.X. Fu, Micropor. Mesopor. Mater. 176 (2013) 48.
[3] L.A. Rocha, M.A. Schiavon, C.S. Nascimento Jr., L. Guimarães, M.S. Góes, A. M. Pires, C.O. Paiva-Santos, O.A. Serra, M.A. Cebim, M.R. Davolos, J.L. Ferrari, J. Alloys Compd. 608 (2014) 73.
[4] S.P. Tiwari, M.K. Mahata, K. Kumar, V.K. Rai, Spectrochim. Acta A 150 (2015) 623.
[5] C. Mayrinck, M.A. Schiavon, C.S. Nascimento Jr., L. Guimarães, M.R. Davolos, M. S. Góes, R.R. Gonçalves, A.M. Pires, S.J.L. Ribeiro, J.L. Ferrari, Ceram. Int. 41 (2015) 1189.
[6] Y. Ledemi, M.E. Amraoui, J.L. Ferrari, P.L. Fortin, S.J.L. Ribeiro, Y. Messaddeq, J. Am. Ceram. Soc. 96 (2013) 825.
[7] C.S. Cunha, J.L. Ferrari, D.C. Oliveira, L.J.Q. Maia, A.S.L. Gomes, S.J.L. Ribeiro, R. R. Gonçalves, Mater. Chem. Phys. 136 (2012) 120.
[8] F.T. Aquino, J.L. Ferrari, S.J.L. Ribeiro, A. Ferrier, P. Goldner, R.R. Gonçalves, Opt. Mater. 35 (2013) 387.
[9] J.L. Ferrari, K.O. Lima, L.J.Q. Maia, S.J.L. Ribeiro, A.S.L. Gomes, R.R. Gonçalves, J. Nanosci. Nanotechnol. 11 (2011) 2540.
[10] L.A. Rocha, S.J.L. Ribeiro, A.C. Pereira, M.A. Schiavon, J.L. Ferrari, Process. Appl. Ceram. 9 (2015) 23.
[11] O.L. Malta, L.D. Carlos, Quim. Nova 26 (2003) 889.
[12] A. Polman, J. Appl. Phys. 82 (1997) 1.
[13] G. Lakshminarayana, M. Mao, R. Yang, J.R. Qiu, M.G. Brik, Physica B 404 (2009) 3348.
[14] F.M.F. Filho, R.R. Gonçalves, S.J.L. Ribeiro, L.J.Q. Maia, Mater. Sci. Eng. B Solid 194 (2015) 21.
[15] J.L. Ferrari, K.O. Lima, E. Pecoraro, R.A.S. Ferreira, L.D. Carlos, R.R. Gonçalves, J. Mater. Chem. 22 (2012) 9901.
[16] D. Manzani, J.L. Ferrari, F.C. Polachini, Y. Messaddeq, S.J.L. Ribeiro, J. Mater. Chem. 22 (2012) 16540.
[17] L.Q. Xiong, Z.G. Chen, M.X. Yu, F.Y. Li, C. Liu, C.H. Huang, Biomaterials 30 (2009) 5592.
[18] J. Zhou, Y. Sun, X. Du, L. Xiong, H. Hu, F. Li, Biomaterials 31 (2010) 3287.
[19] L.F. Johnson, H.J. Guggenheim, Appl. Phys. Lett. 19 (1971) 44.
[20] F. Moglia, S. Müller, F. Reichert, P.W. Metz, T. Calmano, C. Kränkel, E. Heumann, G. Huber, Opt. Mater. 42 (2015) 167.
[21] J. Wang, J. Wu, J. Lin, M. Huang, Y. Huang, Z. Lan, Y. Xiao, G. Yue, S. Yin, T. Sato, Chemsuschem 5 (2012) 1307.
[22] B.M. van der Ende, L. Aarts, A. Meijerink, Phys. Chem. Chem. Phys. 11 (2009) 11081.
[23] R.V. Perrella, D.P. Santos, G.Y. Poirier, M.S. Góes, S.J.L. Ribeiro, M.A. Schiavon, J. L. Ferrari, J. Lumin. 149 (2014) 333.
[24] S. Lv, Z. Zhu, Y. Wang, Z. You, J. Li, C. Tu, J. Lumin. 144 (2013) 117.
[25] J.H. Huang, X.H. Gong, Y.J. Chen, Y.F. Lin, J.S. Liao, X.Y. Chen, Z.D. Luo, Y. D. Huang, Appl. Phys. B 89 (2007) 73.
[26] X. Lu, Z. You, J. Li, Z. Zhu, G. Jia, B. Wu, C. Tu, J. Phys. D: Appl. Phys. 39 (2006) 3755.
[27] M. Haase, H. Schaefer, Angew. Chem. Int. Ed. 50 (2011) 5808.
[28] G. Mialon, S. Tuerkcan, G. Dantelle, D.P. Collins, M. Hadjipanayi, R.A. Taylor, T. Gacoin, A. Alexandrou, J.-P. Boilott, J. Phys. Chem. C 114 (2010) 22449.
[29] D. Zhou, X. Xu, X. Chen, H. Zhu, D. Li, J. Di, C. Xia, F. Wu, J. Xu, Phys. Status Solidi A 209 (2012) 730.
[30] G.C. Kim, T.W. Kim, S.-I. Mho, S.G. Kim, H.L. Park, J. Korean Phys. Soc. 34 (1999) 97.
[31] W.D. Tan, D.Y. Tang, X.D. Xu, D.Z. Li, J. Zhang, C.W. Xu, Z.H. Cong, J. Xu, Laser Phys. Lett. 8 (2011) 193.
[32] E.F. Kustov, V.P. Petrov, D.S. Petrova, Phys. Status Solidi A 41 (1977) 379.
[33] W.E. Langlois, C.C. Shir, Comput. Method Appl. M 12 (1977) 145.
[34] J.C. Souriau, C. Borel, Ch Wyon, C. Li, R. Moncorgé, J. Lumin. 59 (1994) 349.
[35] P. Courty, H. Ajot, C. Marcilly, Powder Technol. 7 (1973) 21.
[36] J.I. Cosimo, C.R. Apesteguía, J. Catal. 116 (1989) 71.

[37] R. Hariharan, P. Gopalan, Solid State Sci. 13 (2011) 168.
[38] R.V. Perrella, C.S. Nascimento Júnior, M.S. Goes, E. Pecoraro, M.A. Schiavon, C. O. Paiva-Santos, H. Lima, M.A. Couto dos Santos, S.J.L. Ribeiro, J.L. Ferrari, Opt. Mater. 57 (2016) 45.
[39] D. Geng, G. Li, M. Shang, C. Peng, Y. Zhang, Z. Cheng, J. Lin, Dalton Trans. 41 (2012) 3078.
[40] M. Rajendran, M.S. Rao, J. Solid State Chem. 113 (1994) 239.
[41] P. Tarte, Spectrochim. Acta 23A (1967) 2127.
[42] P.Y. Jia, J. Lin, X.M. Han, M. Yu, Thin Solid Films 483 (2005) 122.
[43] J.L. Ferrari, K.O. Lima, L.J.Q. Maia, R.R. Gonçalves, Thin Solid Films 519 (2010) 1319.
[44] F. Vetrone, J.C. Boyer, J.A. Capobianco, A. Speghini, M. Bettinelli, J. Appl. Phys. 96 (2004) 661.
[45] F. Auzel, Chem. Rev. 104 (2004) 139.
[46] R.B. Anderson, S.J. Smith, P.S. May, M.T. Berry, J. Phys. Chem. Lett. 5 (2014) 36.
[47] L. Zampedri, G.C. Righini, H. Portales, S. Pelli, G.N. Conti, M. Montagna, M. Mattarelli, R.R. Gonçalves, M. Ferrari, A. Chiasera, M. Bouazaoui, C. Armellini, J. Non-Cryst. Solids 345–346 (2004) 580.
[48] J.L. Ferrari, K.O. Lima, L.J.Q. Maia, S.J.L. Ribeiro, R.R. Gonçalves, J. Am. Ceram. Soc. 94 (2011) 1230.
[49] T.F. Xu, X. Shen, Q.H. Nie, Y. Gao, Opt. Mater. 28 (2006) 241.